Changes in lamina structure are followed by spatial reorganization of heterochromatic regions in caspase-8-activated human mesenchymal stem cells

Vered Raz[1,*], Françoise Carlotti[1], Bart J. Vermolen[2], Egge van der Poel[2], Willem C. R. Sloos[1], Shoshan Knaän-Shanzer[1], Antoine A. F. de Vries[1], Rob C. Hoeben[1], Ian T. Young[2], Hans J. Tanke[1], Yuval Garini[2,3] and Roeland W. Dirks[1]

[1]Department of Molecular Cell Biology, Leiden University Medical Center, Einsteinweg 20, 2300RC Leiden, The Netherlands
[2]Quantitative Imaging group, Department of Applied Sciences Delft University of Technology, Delft, The Netherlands
[3]Department of Physics, Bar-Ilan University, Ramat-Gan 52900, Israel
*Author for correspondence (e-mail: v.raz@lumc.nl)

Summary

Apoptosis is fundamental to the regulation of homeostasis of stem cells in vivo. Whereas the pathways underlying the molecular and biochemical details of nuclear breakdown that accompanies apoptosis have been elucidated, the precise nature of nuclear reorganization that precedes the demolition phase is not fully understood. Here, we expressed an inducible caspase-8 in human mesenchymal stem cells, and quantitatively followed the early changes in nuclear organization during apoptosis. We found that caspase-8 induces alteration of the nuclear lamina and a subsequent spatial reorganization of both centromeres, which are shifted towards a peripheral localization, and telomeres, which form aggregates. This nuclear reorganization correlates with caspase-3 sensitivity of lamina proteins, because the expression of lamin mutant constructs with caspase-3 hypersensitivity resulted in a caspase-8-independent appearance of lamina intranuclear structures and telomere aggregates, whereas application of a caspase inhibitor restrains these changes in nuclear reorganization. Notably, upon activation of apoptosis, we observed no initial changes in the spatial organization of the promyelocytic leukemia nuclear bodies (PML-NBs). We suggest that during activation of the caspase-8 pathway changes in the lamina structure precede changes in heterochromatin spatial organization, and the subsequent breakdown of lamina and PML-NB.

Introduction

Maintenance of the pool of stem cells is under tight control in vivo and is balanced by the rate of cell proliferation, differentiation and apoptosis (Lawen, 2003). During development, apoptosis is triggered by ligand-activated receptors and the initial cytosolic step is the activation of the initiator caspase-8 or caspase-10. The activated initiator caspase releases the effector caspase-3 or caspase-7 from their inactive states by partial proteolysis (reviewed in Boatright and Salvesen, 2003). Finally, the activated effector caspases cleave cellular substrates, leading to membrane blebbing, DNA degradation and nucleus fragmentation (Wyllie et al., 1981; Nagata, 2005). Proteins of the nuclear envelope, which support the nuclear architecture, are directly cleaved by the effector caspases (Lazebnik et al., 1995). Cleavage of the lamina proteins is crucial for cell death because the structural support of the nucleus depends on an intact lamina structure. The lamin B proteins are cleaved by caspase-3 (Lazebnik et al., 1995; Slee et al., 2001), whereas the lamin A/C proteins are cleaved by caspase-6 (Takahashi et al., 1996; Ruchaud et al., 2002). During the nuclear breakdown phase, cleavage of the lamina proteins precedes DNA condensation, which is subsequently fragmented (Rao et al., 1996). Moreover, it was suggested that chromatin condensation during apoptosis depends on

degradation of lamin A (Ruchaud et al., 2002). However, the changes in nuclear organization that precede the nuclear breakdown phase were so far poorly studied.

Biochemical studies revealed dynamic interactions with chromatin-binding proteins (Mattout-Drubezki and Gruenbaum, 2003), therefore it was suggested that lamina proteins, which are present at the nuclear periphery and throughout the nucleoplasm, may play a role in the spatial positioning of chromatin in the nucleus. High-resolution 3D microscopy studies have shown that the chromatin is not randomly organized, but is spatially ordered to allow control of transcriptional programs (Misteli, 2005; Gorski and Misteli, 2005; van Driel et al., 2003; Kim et al., 2004; Arney and Fisher, 2004; Cremer et al., 2004). Also, constitutive heterochromatin regions, which contain non-coding sequences, show dynamic movements. Changes in the preferred distribution of centromeres and telomeres were found during the cell cycle and in differentiated cells (Solovei et al., 2004; Stadler et al., 2004; Wiblin et al., 2005; Weierich et al., 2003; Chuang et al., 2004). Nuclear bodies are sites where nuclear factors and other regulatory proteins accumulate in high concentrations, and serve to enhance the efficiency of enzymatic reactions (Lamond and Sleeman, 2003). Thus, the spatial organization of nuclear bodies also plays a role in nuclear function (Bubulya

and Spector, 2004). Overall, the dynamic nature of this nuclear spatial organization allows local and temporal interactions between chromatin regions and various nuclear compartments that contribute to cell function (Misteli, 2005).

Human mesenchymal stem cells (hMSCs) are maintained by a carefully integrated process of cell renewal, differentiation, senescence and apoptosis. In vivo and ex vivo, hMSCs can replicate as undifferentiated cells and have the potential to differentiate to various lineages of connective-tissue cell types (Pittenger et al., 1999). In recent years, hMSCs have attracted much attention for their potential therapeutic applications (Caplan and Bruder, 2001; Le Blanc and Pittenger, 2005; Pittenger et al., 1999). These cells offer a number of advantages, including the fact that they are primary cells and, consequently, resemble more the in vivo situation. In this study we have used hMSCs, isolated from bone marrow, to study the initial changes in the structure and organization of the nucleus induced by caspase-8. We have used an inducible caspase-8 (Carlotti et al., 2005), which allows studying early events during activation of apoptosis. Activation of caspase-8 leads first to an alteration of the lamina structure and to specific changes in the spatial organization of heterochromatic regions but not of nuclear bodies, like PML-NBs. Using 3D quantitative image analyses, we found that the spatial position of the centromeres is shifted from a central towards a peripheral nuclear localization, while the telomeres formed aggregates. Furthermore, we confirm the findings of previous studies (Broers et al., 2002; Ruchaud et al., 2002), showing that lamina reorganization during activation of apoptosis precedes chromatin breakdown, and we extend these observations by showing that it depends on caspase-3 activation. Moreover, we show that lamina reorganization precedes spatial reorganization of telomeres and centromeres. Thus, we suggest that activation of the caspase-8 pathway induces sequential changes in nuclear organization, where reorganization of the lamina is followed by a characteristic spatial reorganization of heterochromatin and ultimately leads to breakdown of the nucleus.

Results
Expression of caspase-8 lentiviral vectors induces apoptosis in hMSCs
To study apoptosis in hMSCs, we have used the recently described inducible caspase-8, in which the active domain of caspase-8 was fused with a derivative of FKBP12 (Carlotti et al., 2005). This construct is hereafter referred to as FKC8. In the presence of the dimerization inducer AP20187 FKC8 becomes activated. The chimeric gene was expressed in hMSCs using a lentivirus-mediated gene transfer system (Carlotti et al., 2004; Zufferey et al., 1998). Three days after lentivirus transduction, cells were treated with 100 nM AP20187 for 16 hours. The effect of caspase-8 activation was clearly visible as the cellular confluency was reduced from ~70-80% to ~20-30%, and a substantial amount of dead cells appeared (Fig. 1A). Evidence that this reduction was due to apoptosis was provided by both expression of annexin V and presence of DNA degradation (data not shown). Expression of either, constitutively active caspase-8 (CC8) or FKC8, which is activated by AP20187, leads to a significant increase in the number of nuclei with condensed DNA, a prominent feature of apoptosis (Fig. 1B). To demonstrate the specificity of caspase-

8 induction, cells were treated with Z-VAD.fmk, an inhibitor of the caspase pathway (Carlotti et al., 2005). Activation of caspase-8 in the presence Z-VAD.fmk resulted in a significant decrease in the amount of cells showing condensed DNA (Fig. 1B, AP+Z). Cells expressing the FKC8 vector did not show significant cell death without AP20187 treatment (Fig. 1B, FKC8) and the transduced cells continued to grow normally for 7-8 passages. Furthermore, cell death was not observed in cells transduced with a CMV-GFP lentiviral vector (data not shown). These results show that lentiviral vectors efficiently transfer genes into hMSCs, without affecting cell growth in culture. Moreover, apoptosis can be efficiently initiated after activation of FKC8.

It is well established that cleavage of caspase-3 is one of the downstream events elicited by caspase-8 activation. To confirm that our inducible system works, we visualized the cleaved caspase-3, by using an antibody that specifically recognizes the cleaved forms of caspase-3 (Tewari et al., 1995). The two cleaved forms of casaspase-3 were detectable only in caspase-8 activated but not in mock-treated cells (data not shown). To follow activation of apoptosis in cells, non-transduced or FKC8-transduced cells were immunostained for the cleaved caspase-3 or caspase-8. The cleaved caspase-3 was detected only after caspase-8 activation, but not in control cells (Fig. 1C). Following caspase-8 activation, nuclear morphology changed from a round to a convoluted, as indicated by DAPI staining (Fig. 1C +AP20187, DAPI). Finally, the nuclear morphology was completely lost when DNA staining leaked-out from the nucleus and was found in the cytoplasm (Fig. 1C, DAPI). In cells with a round nucleus, cleaved caspase-3 was present in the cytoplasm, whereas in cells with a convoluted nucleus, staining appeared also in the nucleus (Fig. 1C, +FKC8). As expected, caspase-8 immunostaining was clearly visible at the plasma membrane after FKC8 transduction (Fig. 1C, +FKC8). However, after treatment with AP20187, caspase-8 was found at the nuclear periphery (Fig. 1C, +FKC8). In cells that lost their nuclear morphology, both the cleaved-caspase-3 and caspase-8 staining patterns overlapped with DAPI staining of the DNA (Fig. 1C, +FKC8, degraded). In these cells, DAPI staining revealed deformed nuclear DNA. These observations demonstrate that activation of the caspase-8 pathway leads to a relocation of caspases to the nucleus, where they cleave nuclear proteins (Boatright and Salvesen, 2003). Next, we studied the early changes in spatial nuclear organization after activation of the caspase-8 pathway, and we focused on cells with round and convoluted nuclei.

Activation of caspase-8 leads to spatial changes in lamina morphology
To study nuclear lamina organization following caspase-8 activation, we generated lentiviral constructs coding for lamin A coupled to DsRed (lamin A-DsRed), lamin B coupled to green fluorescent protein (lamin B-GFP) and histone H4 coupled to cyan fluorescent protein (histone H4-CFP). When expressed in hMSCs, both lamin A-DsRed and lamin B-GFP localized at the inner nuclear envelope and showed overlapping distribution with the endogenous lamina proteins (data not shown) (see also Broers et al., 1999). The lamina in hMSCs revealed round and flat nuclei (Fig. 2A). For our studies, we selected cells with fluorescence intensities that were comparable with the endogenous counterparts, as revealed by
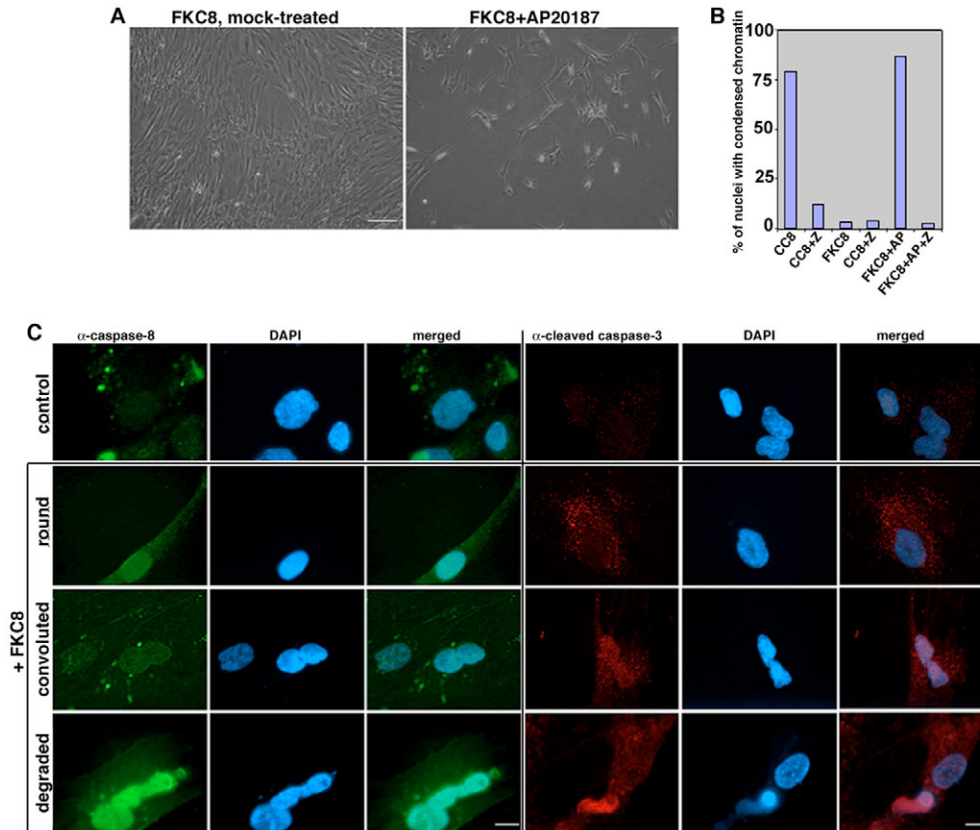
Fig. 1. Induction of apoptosis in hMSCs using lentivirus vector expressing a constitutive (CC8) or an inducible caspase-8 (FKC8). (A) Human MSCs at passage four were transduced with lentivirus vector containing FKC8. Graphs show the cultures before or after treatment with the FKC8 activator AP20187. Bar, 20 μm. (B) Quantification of apoptotic cells after caspase-8 activation. Human MSCs were transduced with CC8 or FKC8. FKC8 was activated with 100 nM AP20187 (+AP) and caspase activity was inhibited with 50 nM Z-VAD.fmk (+Z). Treatments were carried out for 6 hours. Nuclei were stained with DAPI. Histograms show the fraction of cells with condensed DNA as calculated from a population of 250 nuclei. (C) Detection of FKC8-activation pathway using immunostaining. Human MSCs at passage six were transduced with FKC8 followed by AP20187 treatment for 6 hours (+FKC8). Control cells were left non-transduced. Subsequently, cells were fixed and immunostained with anti-caspase-8 (green) or anti-cleaved caspase-3 (red) antibodies. DAPI staining was used to monitor changes in DNA morphology. Nuclear morphology is indicated on the left side. Bars, 10 μm.

immunocytochemistry, and exhibited round nuclei. Human MSCs were first transduced with lamin A-DsRed or lamin B-GFP lentiviral vectors and then with the histone H4-CFP vector. To activate the caspase-8 pathway, these cells were also transduced with the lentiviral vectors FKC8 or CC8. Cells were imaged using confocal microscopy and the collected Z-stacks were processed with TeloView (Vermolen et al., 2005) generating 3D reconstructions. Without caspase-8 activation, hMSCs exhibited round and flat nuclear lamina (Fig. 2A, control, *xy*-axis and *xz*-axis). After treatment with 100 nM AP20187, the spatial organization of the lamina changed dramatically without affecting the staining pattern of histone H4-CFP (Fig. 2A, +AP20187), suggesting that changes in lamina organization precede massive changes in chromatin organization. To determine whether lamina morphology coincides with DNA fragmentation terminal deoxynucleotidyl transferase biotin-dUTP nick-end labeling (TUNEL) staining for detection of DNA fragmentation was combined with lamin B immunohistochmistry. DNA fragmentation was not detected in control cells, where FKC8 had not been activated (Fig. 2B, –AP20187). After activation of FKC8, degraded DNA was

detected only in cells with degraded lamin B (Fig. 2B, long arrows), but not in cells with a convoluted nucleus (Fig. 2B, short arrows).

When hMSCs that express both lamin B-GFP and FKC8 were treated with 10 nM AP20187, lamin B degradation was found after 20 hours, compared with 6 hours when treated with 100 nM AP20187, indicating that the speed of lamin B degradation by caspase-8 can be manipulated by AP20187 concentration. After a 4-hour treatment with 10 nM AP20187, the lamin B-GFP organization was dispersed in a vertical direction, form the nuclear envelope towards the nuclear interior (Fig. 2C +AP, gray image of the *yz*-axis). Some lamina structures were observed inside the nucleoplasm, being disconnected from the lamina structure at the inner nuclear membrane. Generally, a 10-fold to 20-fold increase in the amount of lamin B-GFP in the nuclear interior was found compared with mock-treated cells (Fig. 2A). This change in lamin B-GFP organization was not found in cells treated with 50 nM Z-VAD.fmk (Fig. 2C +AP+Z). Thus, activation of the caspase-8 pathway leads to a spatial reorganization of the lamina structure, which precedes the massive degradation of

lamin A and lamin B proteins. These results confirm previous observations in other cell types, suggesting that degradation of lamina proteins precedes chromatin degradation (Rao et al., 1996).

Since the nuclear lamina provides structural support to the nucleus, changes in lamina organization are expected to affect nuclear dimensions. To investigate this, we measured the nuclear depth of cells expressing both lamin B-GFP and active caspase-8 by using confocal scanning microscopy. A twofold increase in nuclear depth was measured in cells expressing lamin B-GFP and CC8, compared with cells expressing lamin B-GFP only (Fig. 2D). A similar increase in nuclear depth was measured in cells expressing FKC8 after treatment with 100 nM AP20187, whereas treatment with 10 nM AP20187 showed no significant effect on nuclear depth (Fig. 2D, FKC8+AP). These results suggest that the massive change in lamina organization coincides with an increase of nuclear depth. Moreover, the intranuclear dispersal of the lamina

structure precedes massive changes in spatial nuclear organization.

Caspase-8 activation induces changes in centromeres and telomeres spatial organization

Since changes in nuclear depth can influence the spatial organization of intranuclear components, we investigated whether the spatial organization of centromeres and telomeres is remodeled in this process. Telomeres were visualized by the telomere-binding proteins Trf1 or Trf2 (Luderus et al., 1996) fused to DsRed or citrine, respectively, and centromeres by the centromere protein A (CenpA) fused to GFP (CenpA-GFP) (Sugimoto et al., 2000). These proteins were expressed in hMSCs together with FKC8 using lentiviral vectors. Living cells were imaged before (mock-treated) and after caspase-8 activation (+AP20187). 3D reconstructions revealed that the CenpA-GFP localization changed dramatically after caspase-8 activation (Fig. 3A). Therefore, we quantified the changes in
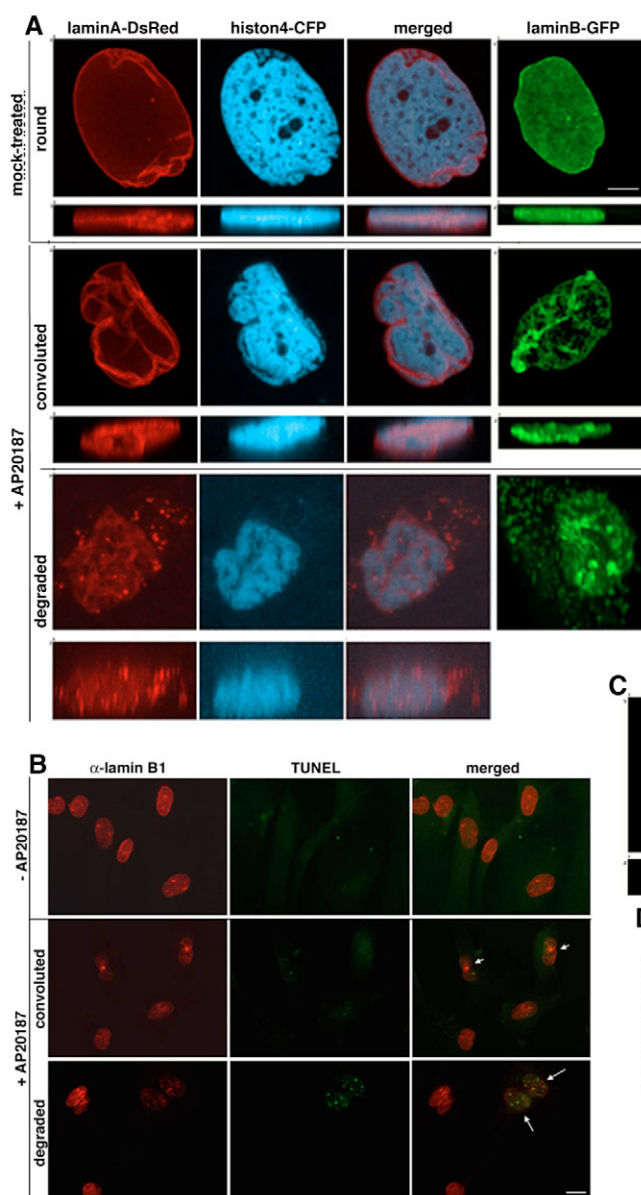

Fig. 2. Changes in lamina morphology during FKC8-induced apoptosis. (A) Human MSCs at passage four were transduced with lentivirus vectors encoding lamin A-DsRed, histone H4-CFP or lamin B-GFP. Cells were finally transduced with FKC8. Control cells were left without AP20187 treatment (mock-treated), and FKC8 was activated by incubating the cells with 100 nM AP20187 for 6 hours. Confocal images were taken from representative nuclei. Images were processed with TeloView and show views of the xy-axis (square) and xz-axis (rectangle) of cells. Bar, 5 μm. (B) Visualization of fragmented DNA and the lamina after FKC8 activation. Cells expressing FKC8 were treated with 100 nM AP20187 for 6 hours or were left without AP20187 treatment. Fragmented DNA (green) was visualized with the Cell Death Detection kit, whereas the lamina was detected with anti lamin B1 antibody (red). Short arrows indicate convoluted nuclei and long arrows indicate nuclei with degraded lamin B. Bar, 10 μm. (C) The effect of Z-VAD.fmk treatment on lamina organization. Human MSCs at passage four were transduced with lamin B-GFP and FKC8 lentiviral vectors. Cells were treated with 50 nM Z-VAD.fmk for two days and 10 nM AP20187 was added during the last 5 hours (+AP+Z). Control cells were treated with 10 nM AP20187 only (+AP). Confocal images were taken from living cells. Images obtained after TeloView processing show maximum projections in xy-axis and xz-axis in green, and a single optical section in the xy-axis in gray. Bar, 5 μm. (D) Statistical analyses of changes in nuclear depth upon caspase-8 activation. Human MSCs at passage four were subsequently transduced with vectors coding for lamin B-GFP and CC8 or FKC8. Control cells were transduced with lamin B-GFP vector only. CC8-transduced cells were examined 16 hours post-transduction. FKC8-transduced cells were treated with either 10 nM or 100 nM AP20187 for 5 hours. Nuclear depth was measured from confocal images. 120 nuclei were evaluated.
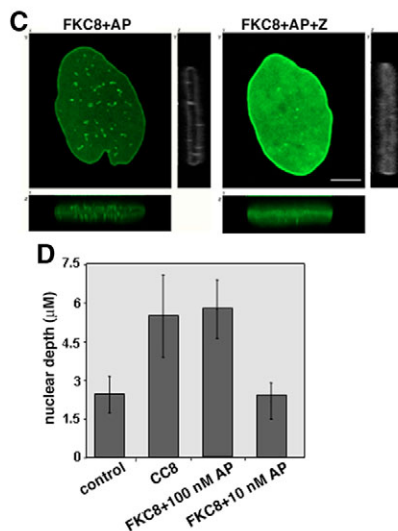
Fig. 3. Centromere spatial localization in FKC8-activated hMSCs. Human MSCs at passage four were transduced with CenpA-GFP followed by FKC8 lentiviral vectors. Confocal images were taken from living cells before (mocked-treated) or 6 hours after 100 nM AP20187 treatment (+AP20187). Images were processed with TeloView. Bar, 5 μm. (A) 3D representation of a nucleus exhibiting a disk or a convoluted morphology. CenpA-GFP is shown in green. DIC image in the *xy*-axis reveals the nuclear rim. Underneath each image, a graph shows the spatial distance of centromeres from the center of mass (CM) after analyses in the algorithm centromeres. (B) Statistical analysis of centromere distribution in FKC8-transduced cells. The spatial localization of CenpA-GFP was evaluated using the centromeres algorithm. The average of CenpA-GFP dots close to center of mass (CM) (0-0.3 normalized distance) or close to the periphery (0.7-1 normalized distance) was calculated. FKC8-transduced cells were treated with 100 nM AP20187 (+AP) only or together with 50 nM Z-VAD.fmk (+AP+Z) for 5 hours. Control cells were mock-treated. AP20187-treated cells were sorted according to nuclear shape (round or convoluted). 50 nuclei were evaluated.
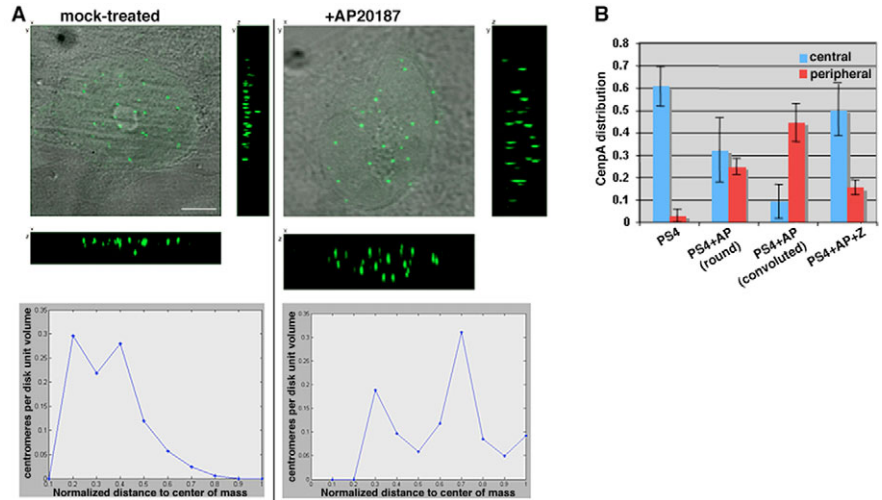
CenpA spatial distribution with a newly developed algorithm (named centromeres, see Materials and Methods). In mock-treated cells, most centromeres were found close to the center of mass of the nucleus (Fig. 3, mock-treated). In AP20187-treated cells, showing a convoluted nuclear shape, most centromeres were found far from the center of mass and some overlapped with the nuclear rim (Fig. 3, +AP20187). This shift in the spatial localization of centromeres was inhibited in the presence of Z-VAD.fmk, because most centromeres were found close to the center of mass (Fig. 3B, PS4+AP+Z). These results further confirm that activation of the caspase-8 pathway leads to a shift in the spatial localization of CenpA. In cells treated with AP20187 showing round nuclei, only half of the centromeres were positioned close to the center of mass, whereas in cells with a convoluted nuclear shape the majority of centromeres were distributed at the periphery (Fig. 3B). These results suggest that the shift in centromere localization coincides with changes in nuclear shape.

Next, we analyzed the spatial organization of telomeres in relation to changes in lamina organization. Trf1-DsRed or Trf2-citrine was expressed in hMSCs together with lamin B-GFP or lamin A-DsRed and with FKC8. In mock-treated cells, the size of Trf1-DsRed or Trf2-citrine fluorescent dots was nearly the same, whereas in AP20187-treated cells, showing a convoluted nuclear shape, small and large fluorescent dots were observed (Fig. 4A). This change in telomere organization was confirmed by the detection of endogenous TRF2 in AP20187-treated cells using immunocytochemistry (data not shown), indicating that the large fluorescent dots are not artifacts introduced by the fusion proteins. These observations suggest that activation of the caspase-8 pathway leads to a spatial reorganization of telomeres. To study the spatial reorganization of telomeres in more detail, the telomere-related fluorescent dots were quantified in TeloView. After sorting and plotting the fluorescent intensities of all Trf1-DsRed dots in individual nuclei from mocked-treated cells, a graph with a single slope was obtained, whereas the graph obtained from AP20187-treated cells showed two different slopes (Fig. 4B,

yellow and green lines, respectively). The graph with the single slope indicates that the variation between the different fluorescent intensities is not significant. However, the graph obtained from AP20187-treated cells with convoluted nuclei shows two distinct slopes. The slope of the low-fluorescence intensities is comparable to the one in the graph obtained from control cells, whereas the slope of the high-fluorescence intensities increases tenfold. This second slope indicates a significant increase in telomere fluorescence intensities and therefore telomere aggregates. This analysis shows that, in hMSCs, telomeres are normally not associated with each other but only after caspase-8 activation some of the telomeres form aggregates. The formation of telomere aggregates might implicate that telomeres are positioned closer to each other after caspase-8 activation. To test this, we measured the spatial distance between every two fluorescent dots in a nucleus using 'TeloDistance' (see Materials and Methods). A 15-fold to 20-fold increase in the percentage of telomeres that were in a close spatial distance was found between mock- and AP20187-treated cells with convoluted nuclei (Fig. 4C). In AP20187-treated cells with round-shaped nuclei two patterns of telomere spatial organization could be distinguished. One pattern was similar to that found in control cells (Fig. 4C, red bars). The second pattern revealed a fourfold increase in the percentage of telomeres in close spatial distance, as well as formation of telomere aggregates (Fig. 4C, blue bars). These aggregates were, however, small because the ratio of fluorescent intensities increased only fourfold in the round nuclei compared with 16-fold in convoluted nuclei (Fig. 4C, green bars). These results further indicate that changes in spatial organization of telomeres succeed changes in lamina structure and suggest a correlation between the two reorganization processes.

To investigate whether the lamina proteins colocalize with telomeres, single digital cross-sections were generated using DIPimage (Hendriks et al., 1999). Cross sections of mock-treated cells (taken from Fig. 4C, yellow bars) revealed no significant overlap between telomeres and the lamins, as

Fig. 4. Spatial organization of telomeres during FKC8-induced apoptosis in hMSCs. (A) Human MSCs at passage four were transduced with lentivirus vectors encoding either Trf2-citrine (shown in green) or Trf1-DsRed (shown in red), followed by a transduction with the lamin A-DsRed (red) or the lamin B-GFP (green) encoding vectors. The cells were finally transduced with FKC8. Confocal images were taken from living cells before (mock-treated) or 4-6 hours after 100 nM AP20187 treatment (+AP20187). Images were processed with TeloView to quantify the fluorescence dots. Images show representative nuclei. Bar, 5 μm. (B) Quantification of telomere fluorescence intensity. The fluorescent dots obtained in A were sorted and plotted according to their intensity. The intensity graph obtained from the control cells is shown in yellow, and that obtained from FKC8-activated cells, showing a convoluted nuclear shape, is shown in green. (C) Statistical analyses of telomere organization. Images of mock-treated or AP20187-treated cells, as described in A, were processed in TeloView. Statistical analyses of Trf1-DsRed spatial organization included the percentage of telomeres in close spatial distance, the percentage of fluorescent particles in aggregates, and the ratio between the two intensity slopes. AP20187-treated cells (+AP) were sorted according to the lamina shape. Forty nuclei were evaluated. (D) DIPimage image analysis shows one optical section along the *xz*-axis of lamin B-GFP-expressing (green) and Trf1-DsRed-expressing (red) cells. Images of representative nuclei within the subclasses, yellow, red, blue and green of C (a, b, c and d, respectively) were processed in DIPimage. Yellow shows overlap between lamin B-GFP and Trf1-DsRed (indicated by arrows). Bar, 5 μm.
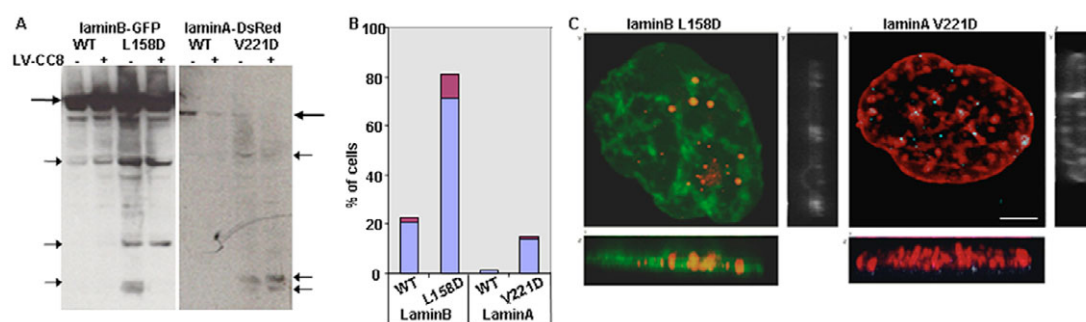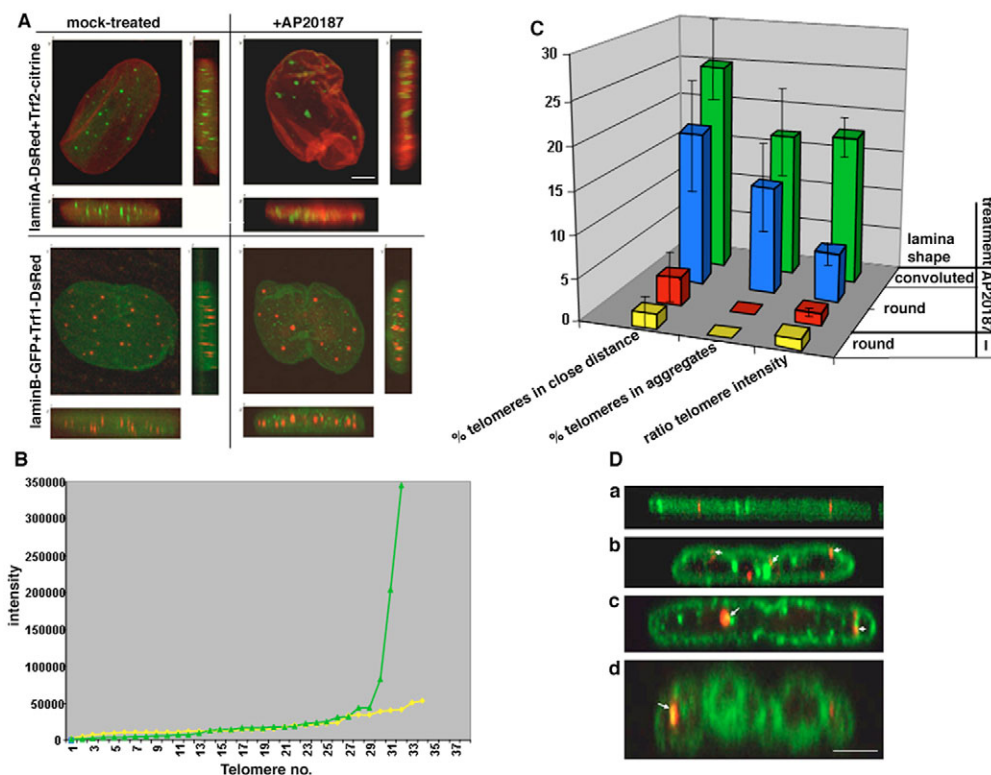

Fig. 5. Mutations in lamin A or lamin B genes that make them caspase-3-sensitive affect lamina and telomere spatial organization. (A) Western blot analysis of lamin degradation in 293T cells. 293T cells were transduced with lentiviral vectors expressing wild-type lamin B-GFP, lamin B-L158D-GFP, wild-type lamin A-DsRed or lamin A V221D-GFP. Subsequently, half of the transformed cells were transduced with LV-CC8 (+). Proteins were extracted 18 hours after transduction and subjected to Western blot analysis. Lamin B-GFP was detected with an anti-GFP antibody and lamin A-DsRed was detected with an anti-lamin A/C antibody. Long arrows indicate the fused protein and small arrows the cleaved products. (B) Quantification of lamina morphologies in hMSCs. Human MSCs at passage four were transduced with lentivirus vectors coding for wild-type lamin B-GFP, lamin B L158D-GFP, wild type lamin A-DsRed, or the lamin A V221D-DsRed. Lamina morphology was determined by fluorescence microscopy. Histograms show the percentage of cells exhibiting intranuclear structures (purple) or degraded (red) lamina structures (as shown in Fig. 2). Maximum projections of confocal images show telomere organization in cells expressing lamin mutants. (C) hMSCs at PS6 were transduced with Trf1-DsRed (red) and lamin B L158D-GFP (green). In cells expressing lamin A V221D-DsRed (red), TRF2 was detected by immunostaining (blue). After TeloView processing, maximum projections in the *xy*-axis and *xz*-axis (in green), and a single section in the *xy*-axis (gray) are shown. Bar, 5 μm.

indicated by the absence of yellow color (Fig. 4Da). In AP20187-treated cells showing lamina intranuclear structures (taken from Fig. 4C, blue and green bars) yellow dots appeared in DIPimage-processed images (Fig. 4Dd,c, indicated by arrows). The yellow color indicates colocalization of lamin B and Trf1. These results suggest that the reorganization of telomeres during activation of the caspase-8 pathway is driven by the intranuclear lamina structure.

Lamina mutants with enhanced sensitivity to caspase-3 affect lamina and telomere spatial organization

So far, we demonstrated that activation of caspase-8 induces alterations in lamina structure that correlate with changes in the spatial organization of telomeres and centromeres. To determine whether activation of the caspase pathway affects the spatial organization of the nucleus directly, we introduced a mutation in the lamin B caspase-3-recognition site VEVD (Zhang et al., 2001). If lamin B is cleaved by caspase-3 only – and/or there is only one caspase-3 site in lamin B – no cleaved products should be found in the VEAD mutant after caspase-8 activation. However, following caspase-8 activation, we found some lamin B cleavage products in hMSCs (data not shown). This result support previous studies in other cell types, showing that a mutation in the VEVD site delays but not abolishes lamin B degradation (Korfali et al., 2004; Zhang et al., 2001). Therefore, to investigate whether changes in lamina structure affect heterochromatin organization, an additional caspase-3 recognition site was introduced into the genes encoding lamin B and lamin A. Although lamin A is normally cleaved by caspase-6 at the conserved VEID site located at amino acids 221-224 (Ruchaud et al., 2002), introduction of a caspase-3 cleavage site into the lamin A gene allows to study the effect of caspase-3 on lamina structure in an unambiguous background. Based on the caspase-3-recognition site DEXD (Thornberry et al., 1997), we introduced a point mutation (V221D) in laminA-DsRed, and a point mutation (L158D) in the lamin B-GFP gene, creating a putative caspase-3-recognition site DEDG. The effect of these mutations on lamina degradation was biochemically studied in HEK293T cells because in these cells higher expression levels can be obtained compared with hMSCs. Western blot analysis revealed the presence of additional cleaved products when lamin B and lamin A mutant constructs were transfected compared with the WT lamin constructs (Fig. 5A), confirming the presence of the caspase-3 recognition site. Cleaved products were found without caspase-8 activation indicating that both mutants were hypersensitive to caspase-3, but activation of caspase-8 resulted in enhanced protein cleavage (Fig. 5A). Interestingly, two of the lamin B cleaved products were hardly detectable after caspase-8 activation. Since caspase-8 activates other effector caspases and previous studies show that lamin B is also a substrate for caspase-7 (Korfali et al., 2004), it is possible that the observed degradation of the cleaved products in the lamin B mutant is carried out by another effector caspase that is activated by caspase-8.

Next, the effect of the mutations was analyzed in lentivirus-transduced hMSCs. The lamin B L158D-GFP and the lamin A V221D-DsRed mutant vectors were located at the inner nuclear envelope, and were co-localized with the endogenous lamin A or lamin B stained by immunocytochemistry (data not shown). Notably, the expression of the mutant lamin proteins

significantly increased the fraction of cells showing deformed lamina morphology, as compared with cells expressing the wild-type lamin vectors lamin B-GFP or lamin A-DsRed (Fig. 5B). Compared with lamin A V221D-DsRed, the expression of lamin B L158D-GFP resulted in a higher percentage of abnormally shaped nuclei. Even without activation of caspase-8, the basal level of caspase-3 activity was sufficient to induce changes in lamina structure, as revealed by the localization of both mutants (Fig. 5C).

Finally, the spatial organization of telomeres was studied in cells expressing lamin B-GFP or lamin A-DsRed mutant vectors. In cells that express the mutant lamin B L158D-GFP and show deformed lamina organization, large fluorescent dots of Trf1-DsRed were found, indicating telomere aggregates (Fig. 5C). The intensity of these large fluorescent dots are similar or sometimes larger compared with the aggregates found in caspase-8-activated cells expressing fluorescent wild-type lamin proteins. Two populations of fluorescence intensity were also found when endogenous TRF2 was detected by immunofluorescence (Fig. 5C right image), although they were much smaller than that of TRF1-DsRed. In cells expressing lamin B L158D-GFP and that exhibited normal round nuclei, no telomere aggregates were found (data not shown). These results suggest a strong correlation between alterations in the spatial organization of lamina and telomere aggregation.

Activation of caspase-8 does not affect distribution of PML-NBs

Our results show that caspase-8 activation induces a spatial reorganization of two heterochromatic structures. Next, we studied whether the spatial organization of other nuclear compartments is also changed. The organization of promyelocytic leukemia nuclear bodies (PML-NBs) is disrupted in apoptotic cells (Bernardi and Pandolfi, 2003; Takahashi et al., 2004; Nacerddine et al., 2005). Therefore, we examined whether the spatial distribution of PML-NBs was also affected at early steps of apoptosis induced by caspase-8. PML-NBs were detected in FKC8-transduced cells expressing CenpA-GFP by using the monoclonal antibody 5E10 (Stuurman et al., 1992). Before activation of the caspase-8 pathway, PML-NBs were positioned in the middle plane of the nucleus similar to centromeres (Fig. 6A, mock-treated). After FKC8 activation, when cell nuclei showed a convoluted morphology and the spatial organization of centromeres changed, the spatial distribution of PML-NBs remained unchanged (Fig. 6A, +AP20187 and Fig. 6B, convoluted). The organization of PML-NBs was only disrupted in apoptotic cells that showed a complete disruption of the lamina structure and contained degraded lamin B-GFP (Fig. 6B).

Discussion

Maintenance of the pools of hMSC involves apoptosis of unwanted cells. To study this process in culture, we made use of an inducible caspase-8 FKC8 (Carlotti et al., 2005). As we demonstrate here, FKC8 is as efficient as the constitutively activated form CC8 in promoting cell death. FKC8 has the ultimate advantage that it is activated on a post-translational level. In addition, we show that the activity of FKC8 can be modulated by the activator AP20187 added at different concentrations to the culture medium. Activation of the apoptotic pathway triggers nuclear breakdown. So far, the
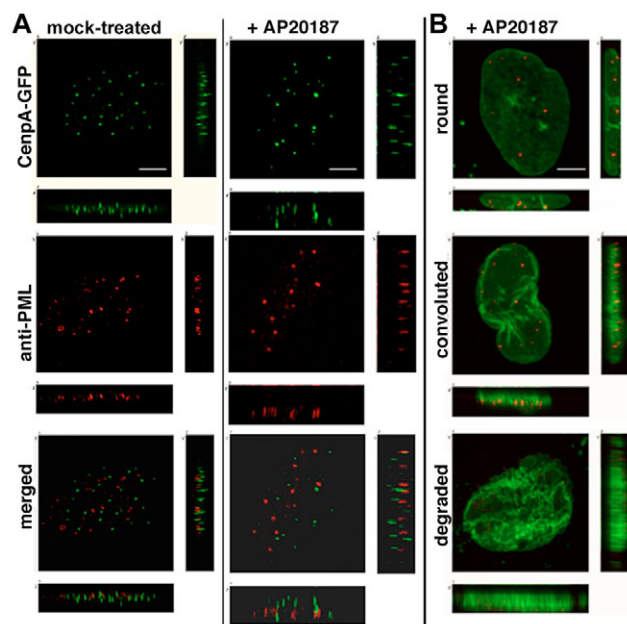
Fig. 6. Spatial organization of PML bodies in caspase-8 activated hMSCs. Human MSCs at passage four were transduced with CenpA-GFP (A) or lamin B-GFP (B), and with FKC8 lentiviral vectors. FKC8 was activated with 100 nM AP20187 for 6 hours (+AP20187). Mock-treated cells were left without AP20187 treatment. Subsequently, cells were subjected to immunostaining using an anti-hPML antibody. Confocal images were processed with TeloView. CenpA-GFP and lamin B-GFP are shown in green and PML is shown in red. Bars, 5 μm.

structural changes that precede the nuclear breakdown have not been fully studied. The inducible FKC8 allows us to study early steps in the caspase-8-induced apoptosis pathway. Moreover, we show that, using lentiviral vectors, we were able to transduce at least three genes in one cell without disrupting the growth of hMSCs.

Our results revealed that upon activation of caspase-8, caspases are relocated to the nucleus where changes in lamina structure are induced, followed by spatial reorganization of telomeres and centromeres. The telomeres formed aggregates, whereas centromeres moved to the nuclear periphery. Previous studies reported changes in the localization of telomeres and centromeres during the cell cycle (Chuang et al., 2004; Solovei et al., 2004) and cell differentiation (Gilchrist et al., 2004; Solovei et al., 2004; Wiblin et al., 2005). It has been suggested that the preferred peripheral localization of centromeres in G0-G1 cells and in some differentiated cells indicate a less-active state of the genome (Cremer et al., 2004). It is, therefore, possible that the peripheral localization of the centromeres, which is induced by the caspase-8 pathway, also indicates genome deactivation. An induced formation of telomere aggregates has been observed in Myc-transformed cells, which eventually resulted in chromosomal rearrangements (Louis et al., 2005). The biological function for telomere aggregation is not yet known. Recent studies, using biochemical approaches, show that telomeric regions are excluded from inter-nucleosomal fragmentation during apoptosis (Schliephacke et al., 2004). Thus, it is possible that, during the onset of

apoptosis, telomere aggregation protects these heterochromatic regions from degradation.

In contrast to the spatial reorganization of telomeres and centromeres, the organization of PML-NBs was initially not affected by caspase-8 activation. Later in the apoptotic process, however, during breakdown of the nucleus, PML-NBs bodies were not detected. This observation is consistent with previous studies showing that PML-NB organization is dramatically disrupted in apoptotic cells (Bernardi and Pandolfi, 2003; Takahashi et al., 2004; Nacerddine et al., 2005). Thus, the caspase-8 pathway initially affects the spatial organization of the lamina and heterochromatic regions, without affecting PML-NBs distribution.

Activation of the caspase-8 pathway induces an increase in intranuclear structures of the lamina, followed by an increase in nuclear depth. Since the nuclear envelope is connected to the cytoskeleton it is possible that the observed increase in nuclear depth results from changes in cytoskeletal regions that are connected with the nucleus. Indeed, recent studies showed that cytoskeletal actin-myosin-based contraction is required for disruption of nuclear integrity during apoptosis (Croft et al., 2005). Thus, it is possible that activation of apoptosis affects first the cytoskeleton, which subsequently affects lamina organization and the formation of interanuclear structures. Then after massive degradation of the lamina results in nuclear breakdown. Degradation of lamina proteins is not specific for caspase-8-induced apoptosis because the intrinsic pathway also triggers degradation of lamina proteins (Broers et al., 2002; Rao et al., 1996). Thus, lamina degradation is a crucial event before DNA degradation and nuclear breakdown can take place. It has been shown that cleavage of lamin A by caspase-6 is required for chromatin condensation (Ruchaud et al., 2002). Moreover, these studies suggest a role for lamin A in organizing the peripheral chromatin. Here, we show that a reorganization of lamin A and lamin B precedes specific changes in the spatial organization of telomeres and centromeres. Using live cell imaging and thin-section image processing, we observed an overlap between intranuclear structures of lamin B-GFP and Trf1-DsRed. Consistent with our results, an association between telomere-binding proteins with lamina proteins has been reported previously (Luderus et al., 1996), and a dynamic interaction between the two was observed during the onset of cell division (Dechat et al., 2004; Scherthan et al., 1996). Thus, we suggest that the change in the intranuclear lamina organization triggers a reorganization of heterochromatic regions during activation of the caspase-8 pathway. However, a direct link between lamina alteration and heterochromatin relocalization needs yet to be demonstrated. Nevertheless, previous studies showed that the correct nuclear envelope localization of the telomeric region of chromosome 4q depends on lamin A/C (Masny et al., 2004). This finding suggests that lamina proteins not only provide structural support to the nucleus but also regulate chromatin spatial organization and, thus, influence chromatin function.

Materials and Methods
Cell culture

immunostaining, cells were seeded on glass dishes. No morphological and growth changes were visible when cells grew on glass for three passages.

HEK293T cells were grown in DMEM without Phenol Red but supplemented with 10% FCS, 1% glutamine and 1% P/S. DNA transfection was carried out with Lipofectamine™ 2000 Reagent (Invitrogen) according to the manufacturer's protocol.

Lentiviruses: construction, production and transduction

Vectors used in our study are the self-inactivating (SIN) vectors, which lose the activity of the promoter located in the 5′ LTR upon replication and integration into the genome of the host cells. The lentiviral vector plasmids derived from the previously described pRRL-CMV (Carlotti et al., 2005), where the expression of the transgene is driven by the cytomegalovirus promoter (CMV). The plasmids pRRL-CMV-CC8 (coding for a constitutive active from of caspase-8) and pRRL-FKC8 (coding for an inducible form of caspase-8) have been previously described (Carlotti et al., 2005). Activation of the inducible caspase-8 was carried out by adding 10 nM or 100 nM AP20187 (ARIAD™) to the growth medium. Caspase activity was inhibited using 50-100 nM Z-VAD.fmk (ICN Pharmaceuticals) (Carlotti et al., 2005).

The pRRL-lamin A-DsRed, pRRL-lamin B1-GFP, pRRL-CenpA-GFP, pRRL-Trf1-DsRed, pRRL histone H4-CFP and pRRL-Trf2-citrine constructs were generated by inserting the coding sequences of the fluorescent proteins into the pRRL-CMV vector. The lamin A-GFP and lamin B-GFP constructs were kindly provided by J. L. V. Broers (Maastricht University, The Netherlands), the hCENPA-GFP construct by W. A. Bickmore (Western General Hospital, Edinburgh, UK), and the CFP-hTRF2 construct by J. M. Zijlmans (Erasmus MC, Rotterdam, The Netherlands). The cDNAs encoding hTRF1 and histone H4 were generated by reverse transcriptase (RT)-PCR and cloned into vectors containing the appropriate fluorescent protein sequence (Clontech Laboratories, Inc).

Virus titers were determined by the p24 elisa kit (Retro-Tek, ZeptoMetrix Corp.). Prior to transduction, hMSCs were washed with EDTA and lentivirus transduction was carried out in the presence of 10 μM DEAE-Dextran. A virus titer in the range of 800-1600 ng p24 per 10^5 cells) was needed to succeed in approximately 30% of cells expressing the fusion proteins, and approximately 80% of cells expressing caspase-8.

To obtain cells expressing two or three different lentiviruses, every lentivirus was separately transduced at intervals of 3-4 days between each transduction. Transduced cells were grown for seven to eight passages without selection pressure and without losing the transgene.

Mutants

Based on the caspase-3 recognition site DEXD (Thornberry et al., 1997), a V221D point mutation was introduced in lamin A-DsRed to create a caspase-3 cleavage site. The mutant was generated by PCR (QuickChange site-directed mutagenesis kit) using the following primers: 5′-GTCATGAGACCCGACTGG**AT**GAGA-TTGACAATGGG-3′ (forward) and 5′-CCCATTGTCAATCTC**AT**CCAGTCGGG-TCTCATGAC-3′ (reverse) to create pRRL-CMV-lamin A V221D-DsRed. Lamin B is a substrate for caspase-3 (Slee et al., 2001) and the caspase-3 recognition site is located at position 228-231 (Zhang et al., 2001). Using the primers 5′-GGTGACAAAAAAAGT**GAT**GAGGGAGATTTGGAG-3′ (forward) and 5′-CTC-CAAATCTCCCTC**AT**CACTTTTTTTGTCACC-3′ (reverse) an extra caspase-3 cleavage site, DEDG, was created to generate pRRL-CMV-lamin B L158D-GFP. Bases is bold indicate mutations. All mutated DNAs were verified by sequencing.

Western blot analyses

Cells were lysed in NuPAGE LDS sample preparation buffer (Invitrogen). Protein samples were then size fractionated on Novex 4-12% BisTris gradient gels using MOPS buffer (Invitrogen) and subsequently transferred onto Hybond-C extra membranes (GE Healthcare) using a submarine system (Invitrogen). Blots were stained for total protein using Ponceau S (Sigma-Aldrich). After blocking with PBT (PBS with 0.1% Tween-20) containing 5% non-fat milk powder, the membranes were incubated with rabbit-anti-GFP antibody (1:500, Roche), mouse-anti-human lamin A (1:500), rabbit-anti human-cleaved caspase-3 (1:100, R&D Systems); mouse-anti-human caspase-8 (1:100, R&D Systems). The secondary antibodies that were used were anti-rabbit (1:2000) and anti-mouse (1:5000) horseradish peroxidase (HRP)-conjugated antibodies (Pierce). Bound antibodies were detected by chemiluminescence using ECL Plus (GE Healthcare).

Immunocytochemistry and detection of apoptosis

The antibodies used for immunocytochemistry are: mouse-anti-human lamin A (1:1000; Santa Cruz); rabbit-anti human-cleaved caspase-3 (1:500; R&D Systems); mouse-anti-human caspase-8 (1:500; R&D Systems); mouse-anti-hTrf2 (1:1000 Imgenex); mouse-anti-hPML 5E10 (1:10) (Stuurman et al., 1992), and the appropriate Alexa Fluor-488- or Alexa Fluor-594-labeled secondary antibodies. Cells grown on microscopic glass plates were washed with PBS and fixed in 2% formaldehyde in PBS for 5 minutes. Subsequently, cells were permeabilized in PBS containing 1% Triton X-100 for 15 minutes, washed three times in PBS, and washed once in PBS containing 0.1% Tween 20 (PBT). Then, cells were incubated for 45 minutes with the first antibody diluted in PBT containing 5% normal serum. After

washing off the first antibody, cells were incubated with the secondary antibody for 30 minutes, washed with PBT, and mounted in Citifluor (Agar Scientific, Ltd) containing 200 μg/ml DAPI (Sigma-Aldrich).

Apoptotic cells were detected with either Annexin V using the ApoAlert AnnexinV-eGFP Apoptosis Kit, (BD Biosciences Clontech), or in a TUNEL assay using the Cell Death Detection kit (Roche). The assays were done according to the protocol s provided by the manufacture with the following modifications; using the ApoAlert AnnexinV-eGFP Apoptosis Kit, DAPI was used for DNA visualization. For the TUNEL assay cells were fixed with 2% formaldehyde in PBS for 10 minutes and directly permeabilized with 1% Triton X-100 in PBS. After incubation with the DNA labeling reagents, cells were incubated with anti-lamin B1 antibody followed by anti-mouse Alexa Fluor-594.

Microscopy and image processing

Fluorescence microscopy was performed with a microscope (model: Axiovert 135TV; Zeiss) equipped with a 100 W mercury arc lamp and a 100× NA 1.3 plan Apo objective. Confocal microscopy was performed with a microscope (model TCS-2; Leica) equipped with an argon/krypton laser and a 100 W mercury arc lamp. Image stacks were acquired with a 100× NA 1.4 plan Apo objective and were analyzed with Leica confocal software. Confocal images were processed with TeloView (Vermolen et al., 2005). This program uses some of the image processing algorithms of DIPImage (Hendriks et al., 1999) developed at the Quantitative Imaging Group (TU-Delft, The Netherlands, http://www.qi.tnw.tudelft.nl/DIPlib), and the image processing toolbox for MatLab (The MathWorks, Natick, MA). For the analyses of the spatial distribution of centromeres, a new algorithm, named centromeres, was developed. The image data from Teloview was converted into a binary image allowing the separation between the background and the centromere objects. The centromere 3D coordinates were determined in relation to the nucleus center of mass. The output of the data is presented in a 2D graph where the normalized number of centromeres per volume unit is plotted against the normalized distance from the center of mass according to the formula:

$$\frac{\left(\dfrac{\text{number of centromeres per class}}{\text{volume of class}}\right)}{\sum\left(\dfrac{\text{number of centromeres per class}}{\text{volume of class}}\right)}.$$

The classes were defined from the equation:

$$\text{stepsize radius} = \frac{\text{maximum distance}}{\text{number of classes}}.$$

The normalizations were necessary to correct for the non-spherical shape of the nucleus. Since the nuclei in hMSCs are elliptic rather than round, the coordinates were corrected for this discrepancy before calculating the distances to the center of mass (for further details: B.J.V., V.R., E.v.d.P., I.T.Y., R.W.D. and Y.G., unpublished).

For spatial analyses of telomere organization, TeloView data was statistically analyzed in Excel. The distance between every two telomeres was calculated for every spot in the cell using TeloDistance. TeloDistance is a macro written in Visual Basic and running in Excel. TeloDistance calculates the distance between the spots using the 3D coordinates that are calculated from the center of gravity of each spot obtained from TeloView. The voxel size was determined from the output image stack obtained from the Leica confocal software and corrected to have an isotropic voxel size in all directions. These coordinates were put into TeloDistance in a dialog box to determine if the distance between every two spots is below a threshold value. The threshold was determined as the average size of the telomeres for each nucleus. The program gives the distances in a matrix where the distance between two spots bellow the threshold is highlighted. The accuracy of the highlighted values was further tested manually.

References

Arney, K. L. and Fisher, A. G. (2004). Epigenetic aspects of differentiation. *J. Cell Sci.* **117**, 4355-4363.

Bernardi, R. and Pandolfi, P. P. (2003). Role of PML and the PML-nuclear body in the control of programmed cell death. *Oncogene* **22**, 9048-9057.

Boatright, K. M. and Salvesen, G. S. (2003). Mechanisms of caspase activation. *Curr. Opin. Cell Biol.* **15**, 725-731.

Broers, J. L., Machiels, B. M., van Eys, G. J., Kuijpers, H. J., Manders, E. M., van Driel, R. and Ramaekers, F. C. (1999) Dynamics of the nuclear lamina as monitored by GFP-tagged A-type lamins. *J. Cell Sci.* **112**, 3463-3475.

Broers, J. L., Bronnenberg, N. M., Kuijpers, H. J., Schutte, B., Hutchison, C. J. and Ramaekers, F. C. (2002). Partial cleavage of A-type lamins concurs with their total disintegration from the nuclear lamina during apoptosis. *Eur. J. Cell Biol.* **81**, 677-691.

Bubulya, P. A. and Spector, D. L. (2004). On the "move"ments of nuclear components in living cells. *Exp. Cell Res.* **296**, 4-11.

Caplan, A. I. and Bruder, S. P. (2001). Mesenchymal stem cells: building blocks for molecular medicine in the 21st century. *Trends Mol. Med.* **7**, 259-264.

Carlotti, F., Bazuine, M., Kekarainen, T., Seppen, J., Pognonec, P., Maassen, J. A. and Hoeben, R. C. (2004). Lentiviral vectors efficiently transduce quiescent mature 3T3-L1 adipocytes. *Mol. Ther.* **9**, 209-217.

Carlotti, F., Zaldumbide, A., Martin, P., Boulukos, K. E., Hoeben, R. C. and Pognonec, P. (2005). Development of an inducible suicide gene system based on human caspase 8. *Cancer Gene Ther.* **12**, 627-639.

Chuang, T. C., Moshir, S., Garini, Y., Chuang, A. Y., Young, I. T., Vermolen, B., van den Doel, R., Mougey, V., Perrin, M., Braun, M. et al. (2004). The three-dimensional organization of telomeres in the nucleus of mammalian cells. *BMC. Biol.* **2**, 12.

Cremer, T., Kupper, K., Dietzel, S. and Fakan, S. (2004). Higher order chromatin architecture in the cell nucleus: on the way from structure to function. *Biol. Cell* **96**, 555-567.

Croft, D. R., Coleman, M. L., Li, S., Robertson, D., Sullivan, T., Stewart, C. L. and Oleson, M. F. (2005). Actin-myosin-based contraction is responsible for apoptotic nuclear disintigration. *J. Cell Biol.* **168**, 245-255.

Dechat, T., Gajewski, A., Korbei, B., Gerlich, D., Daigle, N., Haraguchi, T., Furukawa, K., Ellenberg, J. and Foisner, R. (2004). LAP2{alpha} and BAF transiently localize to telomeres and specific regions on chromatin during nuclear assembly. *J. Cell Sci.* **117**, 6117-6128.

Gilchrist, S., Gilbert, N., Perry, P. and Bickmore, W. A. (2004). Nuclear organization of centromeric domains is not perturbed by inhibition of histone deacetylases. *Chromosome Res.* **12**, 505-516.

Gorski, S. and Misteli, T. (2005). Systems biology in the cell nucleus. *J. Cell Sci.* **118**, 4083-4092.

Kim, S. H., McQueen, P. G., Lichtman, M. K., Shevach, E. M., Parada, L. A. and Misteli, T. (2004). Spatial genome organization during T-cell differentiation. *Cytogenet. Genome Res.* **105**, 292-301.

Knaan-Shanzer, S., van de Watering, M. J. M., van der Velde, I., Goncalves, M. A. F. V., Valerio, D. and de Vries, A. A. F. (2005). Endowing human adenovirus serotype 5 vectors with fiber domains of species B greatly enhances gene transfer into human mesenchymal stem cells. *Stem Cells* **23**, 1598-1607.

Korfali, N., Ruchaud, S., Loegering, D., Bernard, D., Dingwall, C., Kaufmann, S. H. and Earnshaw, W. C. (2004). Caspase-7 gene disruption reveals an involvement of the enzyme during the early stages of apoptosis. *J. Biol. Chem.* **279**, 1030-1039.

Lamond, A. I. and Sleeman, J. E. (2003). Nuclear substructure and dynamics. *Curr. Biol.* **13**, R825-R828.

Lawen, A. (2003). Apoptosis-an introduction. *BioEssays* **25**, 888-896.

Lazebnik, Y. A., Takahashi, A., Moir, R. D., Goldman, R. D., Poirier, G. G., Kaufmann, S. H. and Earnshaw, W. C. (1995). Studies of the lamin proteinase reveal multiple parallel biochemical pathways during apoptotic execution. *Proc. Natl. Acad. Sci. USA* **92**, 9042-9046.

Le Blanc, K. and Pittenger, M. (2005). Mesenchymal stem cells: progress toward promise. *Cytotherapy* **7**, 36-45.

Louis, S. F., Vermolen, B. J., Garini, Y., Young, I. T., Guffei, A., Lichtensztejn, Z., Kuttler, F., Chuang, T. C. Y., Moshir, S., Mougey, V. et al. (2005). c-Myc induces chromosomal rearrangements through telomere and chromosome remodeling in the interphase nucleus. *Proc. Natl. Acad. Sci. USA* **102**, 9613-9618.

Luderus, M. E., van Steensel, B., Chong, L., Sibon, O. C., Cremers, F. F. and de Lange, T. (1996). Structure, subnuclear distribution, and nuclear matrix association of the mammalian telomeric complex. *J. Cell Biol.* **135**, 867-881.

Luengo Hendriks, C. L. and van Vliet L. J. (1999) *in:* M. Boasson, J.A. Kaandorp, J.F.M. Tonino, M.G. Vosselman (eds.), ASCI'99, Proc. 5th Annual Conference of the Advanced School for Computing and Imaging (Heijen, NL, June 15-17), ASCI, Delft, p. 95-102.

Masny, P. S., Bengtsson, U., Chung, S. A., Martin, J. H., van Engelen, B., van der Maarel, S. M. and Winokur, S. T. (2004). Localization of 4q35.2 to the nuclear periphery: is FSHD a nuclear envelope disease? *Hum. Mol. Genet.* **13**, 1857-1871.

Mattout-Drubezki, A. and Gruenbaum, Y. (2003). Dynamic interactions of nuclear lamina proteins with chromatin and transcriptional machinery. *Cell. Mol. Life Sci.* **60**, 2053-2063.

Misteli, T. (2005). Concepts in nuclear architecture. *Bioessays* **27**, 477-487.

Nacerddine, K., Lehembre, F., Bhaumik, M., Artus, J., Cohen-Tannoudji, M., Babinet, C., Pandolfi, P. P. and Dejean, A. (2005). The SUMO pathway is essential for nuclear integrity and chromosome segregation in mice. *Dev. Cell* **9**, 769-779.

Nagata, S. (2005). DNA degradation in development and programmed cell death. *Annu. Rev. Immunol.* **23**, 853-875.

Pittenger, M. F., Mackay, A. M., Beck, S. C., Jaiswal, R. K., Douglas, R., Mosca, J. D., Moorman, M. A., Simonetti, D. W., Craig, S. and Marshak, D. R. (1999). Multilineage potential of adult human mesenchymal stem cells. *Science* **284**, 143-147.

Rao, L., Perez, D. and White, E. (1996). Lamin proteolysis facilitates nuclear events during apoptosis. *J. Cell Biol.* **135**, 1441-1455.

Ruchaud, S., Korfali, N., Villa, P., Kottke, T. J., Dingwall, C., Kaufmann, S. H. and Earnshaw, W. C. (2002). Caspase-6 gene disruption reveals a requirement for lamin A cleavage in apoptotic chromatin condensation. *EMBO J.* **21**, 1967-1977.

Scherthan, H., Weich, S., Schwegler, H., Heyting, C., Harle, M. and Cremer, T. (1996). Centromere and telomere movements during early meiotic prophase of mouse and man are associated with the onset of chromosome pairing. *J. Cell Biol.* **134**, 1109-1125.

Schliephacke, T., Meinl, A., Kratzmeier, M., Doenecke, D. and Albig, W. (2004). The telomeric region is excluded from nucleosomal fragmentation during apoptosis, but the bulk nuclear chromatin is randomly degraded. *Cell Death Differ.* **11**, 693-703.

Slee, E. A., Adrain, C. and Martin, S. J. (2001). Executioner caspase-3, -6, and -7 perform distinct, non-redundant roles during the demolition phase of apoptosis. *J. Biol. Chem.* **276**, 7320-7326.

Solovei, I., Schermelleh, L., During, K., Engelhardt, A., Stein, S., Cremer, C. and Cremer, T. (2004). Differences in centromere positioning of cycling and postmitotic human cell types. *Chromosoma* **112**, 410-423.

Stadler, S., Schnapp, V., Mayer, R., Stein, S., Cremer, C., Bonifer, C., Cremer, T. and Dietzel, S. (2004). The architecture of chicken chromosome territories changes during differentiation. *BMC Cell Biol.* **5**, 44.

Stuurman, N., de Graaf, A., Floore, A., Josso, A., Humbel, B., de Jong, L. and van Driel, R. (1992). A monoclonal antibody recognizing nuclear matrix-associated nuclear bodies. *J. Cell Sci.* **101**, 773-784.

Sugimoto, K., Fukuda, R. and Himeno, M. (2000). Centromere/kinetochore localization of human centromere protein A (CENP-A) exogenously expressed as a fusion to green fluorescent protein. *Cell Struct. Funct.* **25**, 253-261.

Takahashi, Y., Lallemand-Breitenbach, V., Zhu, J. and de The, H. (2004). PML nuclear bodies and apoptosis. *Oncogene* **23**, 2819-2824.

Tewari, M., Quan, L. T., O'Rourke, K., Desnoyers, S., Zeng, Z., Beidler, D. R., Poirier, G. G., Salvesen, G. S. and Dixit, V. M. (1995) Yama/CPP32 beta, a mammalian homolog of CED-3, is a CrmA-inhibitable protease that cleaves the death substrate poly(ADP-ribose) polymerase. *Cell*. **81**, 801-809.

Thornberry, N. A., Rano, T. A., Peterson, E. P., Rasper, D. M., Timkey, T., Garcia-Calvo, M., Houtzager, V. M., Nordstrom, P. A., Roy, S., Vaillancourt, J. P. et al. (1997). A combinatorial approach defines specificities of members of the caspase family and granzyme B. Functional relationships established for key mediators of apoptosis. *J. Biol. Chem.* **272**, 17907-17911.

van Driel, R., Fransz, P. F. and Verschure, P. J. (2003). The eukaryotic genome: a system regulated at different hierarchical levels. *J. Cell Sci.* **116**, 4067-4075.

Vermolen, B. J., Garini, Y., Mai, S., Mougey, V., Fest, T., Chuang, T. C., Chuang, A. Y., Wark, L. and Young, I. T. (2005). Characterizing the three-dimensional organization of telomeres. *Cytometry A* **67**, 144-150.

Weierich, C., Brero, A., Stein, S., von Hase, J., Cremer, C., Cremer, T. and Solovei, I. (2003). Three-dimensional arrangements of centromeres and telomeres in nuclei of human and murine lymphocytes. *Chromosome Res.* **11**, 485-502.

Wiblin, A. E., Cui, W., Clark, A. J. and Bickmore, W. A. (2005). Distinctive nuclear organisation of centromeres and regions involved in pluripotency in human embryonic stem cells. *J. Cell Sci.* **118**, 3861-3868.

Wyllie, A. H., Beattie, G. J. and Hargreaves, A. D. (1981). Chromatin changes in apoptosis. *J. Histochem.* **13**, 681-692.

Zhang, D., Beresford, P. J., Greenberg, A. H. and Lieberman, J. (2001). Granzymes A and B directly cleave lamins and disrupt the nuclear lamina during granule-mediated cytolysis. *Proc. Natl. Acad. Sci. USA* **98**, 5746-5751.

Zufferey, R., Dull, T., Mandel, R. J., Bukovsky, A., Quiroz, D., Naldini, L. and Trono, D. (1998). Self-inactivating lentivirus vector for safe and efficient in vivo gene delivery. *J. Virol.* **72**, 9873-9880.